Low-temperature magnetic structure of $FeSn_2$

G. Venturini and B. Malaman
Laboratoire de Chimie du Solide Minéral, Université de Nancy I, Boite Postale 239, 54506 Vandoeuvre les Nancy Cedex, France

G. Le Caër
Laboratoire de Science et Génie des Matériaux Métalliques, Ecole des Mines, 54042 Nancy Cedex, France

D. Fruchart
Laboratoire de Cristallographie, Centre National de la Recherche Scientifique, 166X, 38042 Grenoble Cedex, France

(Received 25 September 1986)

$FeSn_2$ is a collinear antiferromagnet between $T_N = 378$ K and $T_t = 93$ K as shown by previous neutron diffraction and ^{119}Sn Mössbauer studies. Below T_t, two different noncollinear antiferromagnetic structures are consistent with neutron diffraction results, one, called structure I, being canted along with c axis and the other, denoted structure II, being canted in the basal plane (001) along the [110] direction of the chemical cell of $FeSn_2$. On the other hand, two magnetic structures canted in the basal plane, II^a and II^b, which differ only in the propagation vector agree with ^{119}Sn Mössbauer spectra. The simultaneous use of the two techniques has allowed an unambiguous choice of structure II^a which is simply characterized by a combination of the magnetic couplings observed in the high-temperature magnetic structures of $FeSn_2$ and $MnSn_2$.

I. INTRODUCTION

Iron stannide $FeSn_2$ has a tetragonal $CuAl_2$-type structure (Fig. 1). This compound is antiferromagnetic below $T_N = 378 \pm 2$ K and a second transition occurs at $T_t = 93 \pm 1$ K. The magnetic structure, determined by neutron diffraction,[1] is collinear between T_N and T_t and is characterized by ferromagnetic planes (100) antiferromagnetically coupled along the [100] direction [Fig. 2(a)]. The spin direction is close to [100] at room temperature and it deviates slightly when the temperature decreases to T_t^2. Below T_t the proposed structure is alternately canted from the [110] direction along the c axis[1] [Fig. 2(b)]. In both cases the iron spins lie in the (001) planes.

The $MnSn_2$ and $FeSn_2$ compounds have been studied using ^{119}Sn Mössbauer spectroscopy.[2,3] The ^{119}Sn transferred fields are partially or totally anisotropic in $MnSn_2$ and $FeSn_2$,[2,3] according to the magnetic tin sites. The anisotropic field is related to the existence of covalent bonding between Sn and the first $3d$-metal neighbors (M=Fe or Mn). A field model has been calculated; it accounts quantitatively for the observed fields in $MnSn_2$ and above T_t in $FeSn_2$.[2,3]

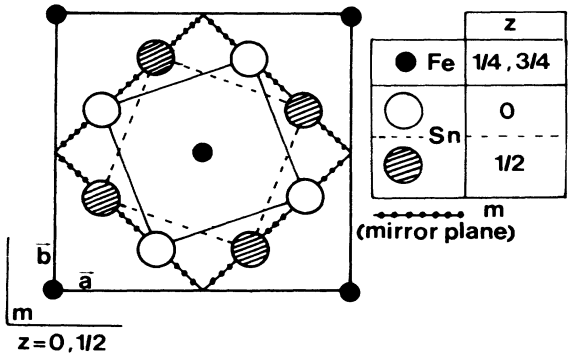

FIG. 1. Basal plane projection of the $FeSn_2$ structure.

Below T_t, it has not been possible to satisfactorily fit the ^{119}Sn Mössbauer spectra using the magnetic structure deduced from neutron diffraction.[1] It has thus been concluded that some local isotropic contributions to the fields must exist below T_t.

We have, therefore, searched for a different magnetic structure model using the low-temperature data of $FeSn_2$. This structure, described in Sec. III, has been constructed in agreement with the ^{119}Sn Mössbauer spectra (Sec. V) and leads to a new explanation for the neutron diffraction data (Sec. IV).

II. CRYSTALLOGRAPHIC STRUCTURE

$FeSn_2$ has the $C16$ structure[4] and symmetry group with $I4/mcm$, with $a = 6.537(2)$ Å, $c = 5.316(2)$ Å. Fe atoms occupy the $4(a)$ $(0,0,\frac{1}{4})$ site while Sn atoms occupy the $8(h)$ $(x,\frac{1}{2}+x,0)$ site with $x = 0.1611(1)$.[5] Fe atoms form chains parallel to the c axis. Each Fe atom is at the center of a square antiprism formed by Sn atoms. Each Sn atom has four Fe nearest neighbors that belong to two neighboring chains at a distance $d = 2.790(2)$ Å. The electric field gradient (EFG) tensor at the Sn sites has its principal axes in the (001) basal plane along the [110] or [1$\bar{1}$0] directions.[2,3]

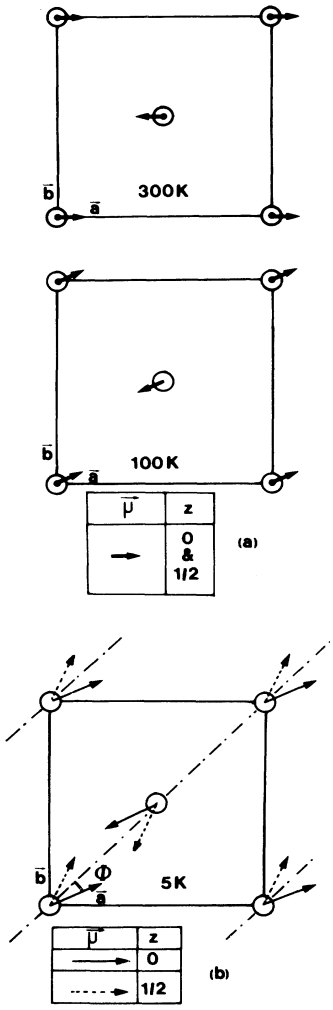

FIG. 2. Magnetic structures of $FeSn_2$ (Ref. 1) (structures I). The spins lie in the (001) plane: (a) Above T (=93 K), structure I^a; (b) at 5 K, structure I^b.

III. MAGNETIC STRUCTURES

A. $T_N < T < T_t$

The magnetic structure, described in Sec. I, is shown in Fig. 2(a). As indicated by ^{57}Fe and ^{119}Sn Mössbauer spectroscopy,[2] a continuous rotation of the local antiferromagnet (AF) easy axis initially [100], takes place in the (001) plane when the temperature decreases. At 100 K, the spins make an angle of 18.5°±4° with the [100] direction.[2]

B. $T < T_t$

The noncollinear antiferromagnetic arrangement proposed in Ref. 1 is shown in Fig. 2(b) and will hereafter be referred to as structure I. The iron moments form a canted structure in the basal plane, the deviation from the [110] direction alternating along the c axis.

^{119}Sn Mössbauer spectra disagree with structure I (Secs. I and V). However, a noncollinear structure is needed to explain the transferred hyperfine fields calculated from such spectra.[2] Therefore, we have tried to find new magnetic structures (referred to hereafter as structures II) with a propagating vector lying in the basal plane (001).

In the high-temperature (HT) range, the hyperfine field of one of the two tin sites, observed in $MnSn_2$ for $T > T_{cr} \approx 73$ K, includes an isotropic contribution.[3]

Taking this into account and combining the magnetic coupling as observed in $MnSn_2$ ($T > T_{cr}$) and $FeSn_2$ ($T > T_t$), we have built a simple magnetic structure canted in the basal plane.

Figure 3(a) represents the proposed model of the low-temperature magnetic structure of $FeSn_2$: structure II^a,

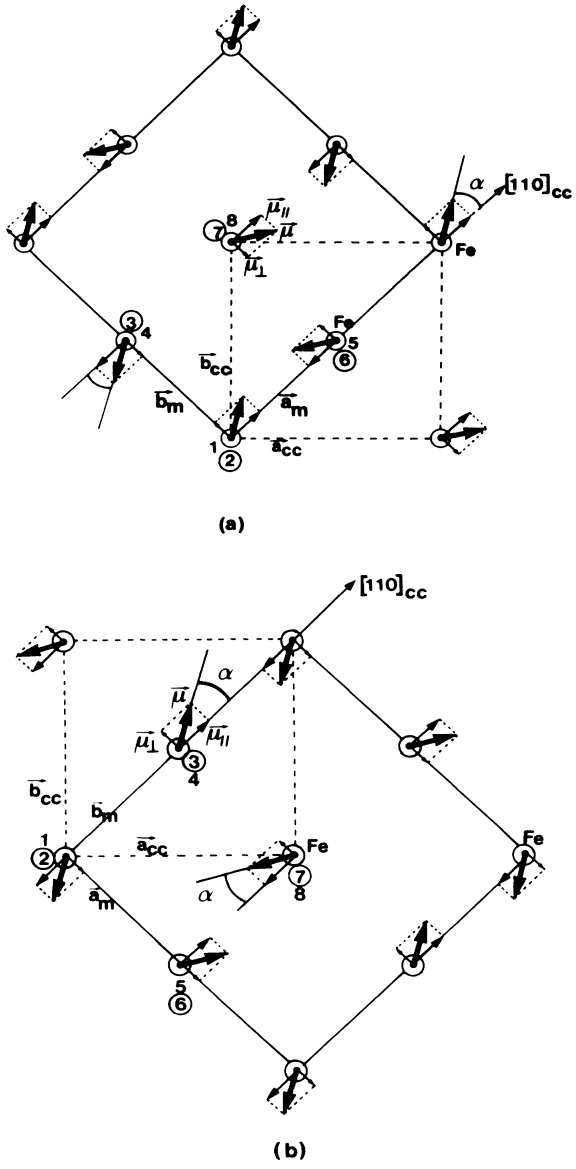

FIG. 3. Magnetic structure models. The spins lie in the (001) plane: (a) structure II^a; (b) structure II^b (to simplify the drawing, the canting direction is chosen as $[110]_{cc}$).

with $[110]_{cc}$ (cc denotes chemical cell) as the main axis of the canting direction as deduced from neutron diffraction and Mössbauer spectroscopy (Sec. IV and V). In this case, the canting angle α corresponds to the angle Φ of Ref. 1.

Comparison of this model with the collinear HT models of $FeSn_2$ [Fig. 2(a)] and $MnSn_2$ [Fig. 3(a) of Ref. 3], can be made by considering the projections $\mathbf{s}_{\parallel}$ and $\mathbf{s}_{\perp}$ of the spins on $[110]_{cc}$ and perpendicular to this axis, respectively: The components $\mathbf{s}_{\parallel}$ form ferromagnetic (100) [and (010)] sheets ordered antiferromagnetically along $[100]_{cc}$ (and $[010]_{cc}$) (as in $FeSn_2$); the components $\mathbf{s}_{\perp}$ form ferromagnetic $(\bar{1}10)$ sheets ordered antiferromagnetically along $[\bar{1}10]_{cc}$ (as in $MnSn_2$).

Another model, structure II^b [Fig. 3(b)], where the components $\mathbf{s}_{\perp}$ form (110) ferromagnetic sheets with the spins lying in this plane (instead of perpendicular to it as in structure II^a) can also be considered. As we will see later, this model disagrees with neutron diffraction data.

In both cases the magnetic cell (m) length is twice the chemical cell (cc) length

$$a_m = a_{cc}\sqrt{2}, \quad c_m = c_{cc} .$$

IV. NEUTRON DIFFRACTION STUDY: A NEW ANALYSIS OF THE EXPERIMENTAL RESULTS

In a previous paper,[1] we deduced the following.

(i) A simple AF collinear structure was only stable between T_N and T_t.

(ii) At lower temperature, a rotation of the easy axis may occur in the (001) plane. But a canted structure was established at very low temperature with an angle $2\phi = 18°$ between $\mathbf{S}(R)$ and $\mathbf{S}(R+\frac{1}{2})$, the main axis being $[110]_{cc}$ (structure I^b in Fig. 2).

Support for this canted model I^b was given by the following.

(i) The rise for $T < 93$ K of new weak magnetic lines, fairly well indexed in the chemical cell as $h+k = 2n+1$. A simple linear deviation of the structure factors in terms of spin components indicates the deviation from collinearity.

(ii) The previously proposed canted magnetic structure for the isotypic compound $FeGe_2$.[6]

(iii) The good agreement of the calculated intensities with respect to the measured ones.

Nevertheless, as indicated in Secs. I and III, the ^{119}Sn Mössbauer spectra do not fit the proposed I^b model at $T < 93$ K.

The new magnetic structure (model II^a, Sec. III) must account for a valuable indexation and existence rules for the observed lines and must yield correct agreement between observed and calculated intensities, including the effect of canting as also detected by Mössbauer spectroscopy.

At the present time, it can be noted that $FeSn_2$ exhibits a very single property which can be related to the particular values of the radii of the elements in such a tetrahedrally close-packed structure; the experimental ratio $a_{cc}/c_{cc} \simeq 1.230$ is very close to $\sqrt{3/2} \simeq 1.225$. This fact allows the possibility of different sets of indices for the lines of a powder pattern, resulting is the ambiguity of different possible "homometric" (in terms of inequivalent magnetic sites) magnetic structures.

TABLE I. Coordinates and magnetic couplings of the iron atoms involved by model II^a [see also Fig. 3(a)] (F, ferromagnetic; AF, antiferromagnetic).

Site	Coordinate x	y	z		Magnetic coupling	
1	0	0	0	S_1	F	AF
2	0	0	$\frac{1}{2}$	S_2		
3	0	$\frac{1}{2}$	$\frac{1}{2}$	S_3	F	
4	0	$\frac{1}{2}$	0	S_4		
5	$\frac{1}{2}$	0	0	S_5	F	AF
6	$\frac{1}{2}$	0	$\frac{1}{2}$	S_6		
7	$\frac{1}{2}$	$\frac{1}{2}$	$\frac{1}{2}$	S_7	F	
8	$\frac{1}{2}$	$\frac{1}{2}$	0	S_8		

The magnetic structure factor can be written in the new cell [Sec. III B, Fig. 3(a)]:

$$\mathbf{F}_{hkl} \propto [1+(-1)^l][1-(-1)^k][\mathbf{s}_1+(-1)^h\mathbf{s}_5] \quad (1)$$

with the numbering of Table I.

In such a way one has to observe systematic extinction for $l = 2n+1$ and for $k = 2n$. But the situation seems rather complicated with the observed lines $(101)_{cc}$, $(301)_{cc}$, and $(103)_{cc}$, "*a priori*" forbidden in the new indexation as $(111)_m$, $(331)_m$, and $(113)_m$, respectively. However, Table II reveals that to their Bragg angle correspond the permitted lines $(210)_m$, $(032)_m$, and $(412)_m$, respectively. The particular relationship between a_{cc} and c_{cc} renders almost impossible discriminating experimentally between the alternative indexation.

Finally, the systematic absence of $(0k0)$ (Table III) can be justified by the vectorial nature of the structure factor, i.e., any geometrical resultant of spins must be directed along $[010]_m$. Model II^b [Fig. 3(b)] cannot satisfy the latter requirement and the calculated magnetic lines $(0k0)$, while relatively weak, should be observed experimentally (due to their enhancement by the Lorentz factor) (Table III).

The final reliability factor for model II^a is $R = 0.03$ (Table III), with a magnetic moment $\mu_{Fe} = (1.70 \pm 0.05)\mu_B$ at 5 K and $(1.68 \pm 0.05)\mu_B$ at 72 K, deviated by $\alpha = 19 \pm 7°$

TABLE II. Equivalence of the indices of the magnetic lines corresponding to models II^a and I^b, respectively.

Model II^a (hkl)	θ (deg)	Model I^b (hkl)	θ (deg)
$(210)_m$	17.80	$(101)_{cc}$	17.83
$(111)_m$[a]	17.80		
$(032)_m$	38.86	$(301)_{cc}$	38.81
$(331)_m$[a]	38.81		
$(412)_m$	47.48	$(103)_{cc}$	47.57
$(113)_m$[a]	47.57		

[a] "*a priori*" forbidden by Eq. (1) (see Sec. IV).

TABLE III. Observed (Ref. 1) and calculated magnetic intensities at 5 and 72 K. Values with an asterisk are comparison between models II[a] and II[b].

	5 K			72 K		
		Model II[a]	Model II[b]		Model II[a]	Model II[b]
hkl	I_0	I_c		I_o	I_c	
010*	0.0	0.0	1.40	0.0	0.0	0.95
110	5.42(0.10)	5.57	5.60	5.28(0.15)	5.36	5.34
210	0.57(0.30)	0.90	0.45	0.60(0.30)	0.89	0.31
130	7.91(0.25)	7.64	7.68	7.9(0.30)	7.35	7.33
310						
030*	0.0	0.0	0.95	0.0	0.0	0.64
112	12.14(0.50)	12.04	12.11	11.80(0.55)	11.58	11.55
410	1.50(1.20)	1.90	2.15	1.00(1.00)	1.88	1.46
212						
330	3.47(0.60)	2.75	2.76	3.22(0.70)	2.64	2.63
032	0.72(1.00)	0.33	1.15	0.70(1.00)	0.32	0.78
312	14.75(0.40)	14.43	14.51	13.60(0.40)	13.88	13.85
132						
430	0.30(1.00)	0.93	2.00	0.30(1.00)	0.92	1.35
232						
150	3.50(1.30)	3.95	3.98	3.00(2.00)	3.80	3.80
510						
050*	0.0	0.0	0.49	0.0	0.0	0.33
412	1.00(10.00)	0.78	0.74	0.50(1.00)	0.77	0.50

from the $[100]_m$ direction [Fig. 3(a)]. We note that the magnetic moment is almost identical to the value calculated from the previous model I[b] (Ref. 1) $[(1.65\pm0.05)\mu_B]$, since in both cases the magnetic structure factors could be expressed as simple arithmetic relations between two noncollinear spins [see Eq. (1) and Table I].

V. MÖSSBAUER STUDIES

A. Hyperfine field model

In Refs. 1 and 2, a hyperfine field model including isotropic and anisotropic terms was successfully used to explain the Sn fields in $MnSn_2$ and $FeSn_2$ above T_t. Furthermore, this field model has been experimentally proved in $FeSn_2$ above T_t when analyzing the ^{57}Fe and ^{119}Sn Mössbauer spectra recorded on a pseudo-single-crystal (see Sec. V B 1) under external magnetic fields: The ^{119}Sn hyperfine field direction was shown to be perpendicular to the direction of the iron magnetic moment.[7]

In the model the ^{119}Sn transferred hyperfine field is written as

$$\mathbf{H}=A_a\sum_{i=1}^{4}\hat{\mathbf{u}}_i(\boldsymbol{\mu}_i\cdot\hat{\mathbf{u}}_i)-\tfrac{1}{3}A_a\sum_{i=1}^{4}\boldsymbol{\mu}_i+\sum_{j(>1)}A_j^{is}\left[\sum_{l=1}^{4}\boldsymbol{\mu}_{jl}\right]. \quad (2)$$

In Eq. (2) the transferred interaction related to a covalency effect is calculated along each Sn—M (M=Fe,Mn) bond as explained in Refs. 1 and 2. $\hat{\mathbf{u}}_i$ is a unit vector directed along each Sn—M bond and $\boldsymbol{\mu}_i$ is the magnetic moment of the corresponding M first nearest neighbor of the Sn atom. The first two terms of Eq. (1) are related to the anisotropic part of the field while the last term is the isotropic contribution of the various M shells around the Sn atom under consideration.

Let us consider the model of Fig. 4 which is structure II[a] with a canting direction (Δ) making an angle β with the $[010]_m$ direction and a canting angle α. Four tin sites, in equal proportions, A, B, C, and C' are expected for this magnetic structure (Fig. 4).

If we define

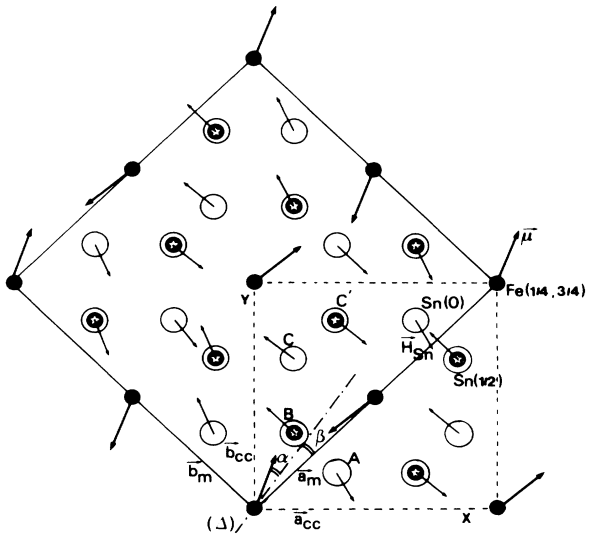

FIG. 4. Low-temperature magnetic structure of $FeSn_2$ (II[a]). The iron magnetic moment directions and the tin hyperfine field directions are shown by arrows.

$$h_0 = 2A_a \frac{a^2}{d^2}\left(\tfrac{1}{4}-x\right) , \tag{3}$$

where a, d, and x have been defined in Sec. II, $A_a = (20.3 \pm 1.7 \text{ kG})\mu_B^{-1}$ (Ref. 2) and

$$\begin{aligned} \mu_1 &= \mu_{\parallel} = \mu \cos\alpha , \\ \mu_2 &= \mu_{\perp} = \mu \sin\alpha , \\ D &= \frac{8x\left(\frac{1}{2}-x\right)}{1-4x} , \\ E &= \frac{4[x^2+(\frac{1}{2}-x)^2]}{1-4x} , \\ \gamma &= \frac{\pi}{4}+\beta , \end{aligned} \tag{4}$$

then Eq. (2) yields

$$\begin{aligned} H_A^x &= h_0(\mu_1\cos\gamma + D\mu_2\cos\gamma - E\mu_2\sin\gamma) - h'_{\text{iso}}\mu_2\sin\gamma , \\ H_A^y &= h_0(-\mu_1\sin\gamma - D\mu_2\sin\gamma + E\mu_2\cos\gamma) + h'_{\text{iso}}\mu_2\cos\gamma , \end{aligned} \tag{5}$$

$$\begin{aligned} H_B^x &= h_0(-\mu_1\cos\gamma + D\mu_2\cos\gamma - E\mu_2\sin\gamma) - h'_{\text{iso}}\mu_2\sin\gamma , \\ H_B^y &= h_0(\mu_1\sin\gamma - D\mu_2\sin\gamma + E\mu_2\cos\gamma) + h'_{\text{iso}}\mu_2\cos\gamma , \end{aligned} \tag{6}$$

where $H_{A,B}^x$ and $H_{A,B}^y$ are the components of the fields $\mathbf{H}_A$ and $\mathbf{H}_B$ in the xy reference frame (see Fig. 4); $h'_{\text{iso}} = h_{\text{iso}} - \frac{4}{3}A_a$, where h_{iso} reflects the isotropic contribution to $\mathbf{H}_A$ and $\mathbf{H}_B$. For sites C and C' the hyperfine fields are both equal to

$$H_C = H_{C'} = H_0 = h_0\mu . \tag{7}$$

As will be seen in Sec. V C, the z principal axis of the electric field gradient (EFG) tensor is along $[110]_{cc}$ ($[010]_m$) for sites A and B (see Fig. 4) as in $MnSn_2$ (direction X_2 of Ref. 3).

The angles θ of the hyperfine field directions with the z principal axes are

$$\begin{aligned} \theta_C &= \alpha+\beta , \\ \theta_{C'} &= |\beta-\alpha| , \end{aligned} \tag{8}$$

for sites C and C' (Fig. 4, see Fig. 8 of Ref. 2).

In the particular case of $\beta=0$, only three tin sites with relative proportions 1:1:2 are expected. Their fields are

$$\begin{aligned} |H_A| &= \mu\,|h_0[\cos\alpha - (1-4x)\sin\alpha] - h'_{\text{iso}}\sin\alpha| , \\ |H_B| &= \mu\,|h_0[\cos\alpha - (1-4x)\sin\alpha] + h'_{\text{iso}}\sin\alpha| , \\ H_C &= h_0\mu , \end{aligned} \tag{9}$$

with angles $\theta_A = \theta_B = 90°$ while $\theta_C\ (=\theta_{C'}) = \alpha$.

B. ^{57}Fe and ^{119}Sn Mössbauer spectroscopy

1. ^{57}Fe

Two ^{57}Fe Mössbauer spectra (Fig. 5) have been recorded at 4.2 and 80 K using a pseudo-single-crystal (PSC) sample obtained by arranging needles side by side. All the needles have their c axis in the sample plane and their

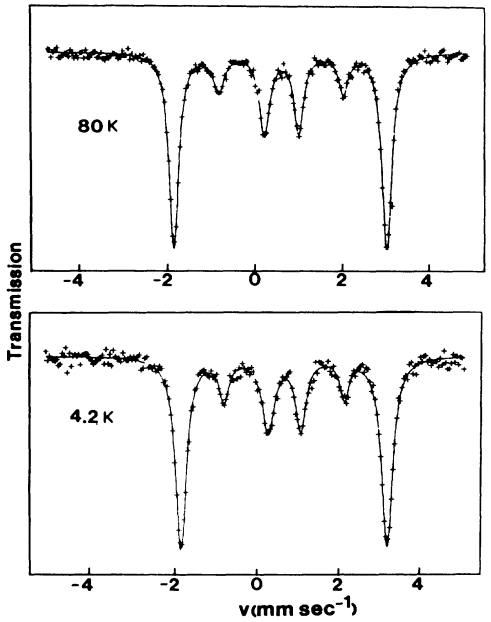

FIG. 5. ^{57}Fe pseudo-single-crystal Mössbauer spectra at 4.2 and 80 K. (The $[110]_{cc}$ directions are parallel to the γ beam.)

$[110]_{cc}$ directions perpendicular to it.

Labeling the peaks from 1 to 6 in order of increasing velocity we define

$$r = (A_2 + A_5)/(A_3 + A_4) , \tag{10}$$

where A_j is the area of the peak j. These ratios are $r = 0.50 \pm 0.12$ and 0.48 ± 0.13 at 4.2 and 80 K, respectively. Then, using the model of Fig. 4 we deduce (from these measurements) a relation which must be obeyed by α and β:

$$r = \frac{4[\sin^2(\alpha+\beta)+\sin^2(\alpha-\beta)]}{[2+\cos^2(\alpha+\beta)+\cos^2(\alpha-\beta)]} \tag{11}$$

and consequently,

$$\sin^2\alpha\cos^2\beta + \sin^2\beta\cos^2\alpha = \frac{2r}{4+r} . \tag{12}$$

Equation (12) will be used as a constraint when analyzing the results of the ^{119}Sn spectroscopy.

We note that if $\beta=0$ (respectively, α) then $\alpha_{\max} = 28° \pm 3°$ and $27° \pm 4°$ (respectively, $\beta_{\max}$) at 4.2 and 80 K, respectively. Moreover, Eq. (12) restricts ranges of variation of α and β between 0 and $\alpha_{\max} = \beta_{\max}$.

2. ^{119}Sn

Figure 6 shows some of the ^{119}Sn spectra recorded below T_t. The higher field (corresponding to the outer peak) increases rapidly between T_t and 77 K and then remains constant between 56 and 4.2 K. Using the model previously proposed (Sec. V A) we have fitted the spectra assuming four different tin sites. However, as sites C and C' differ only in their parameters, θ_C and θ_C, in a first

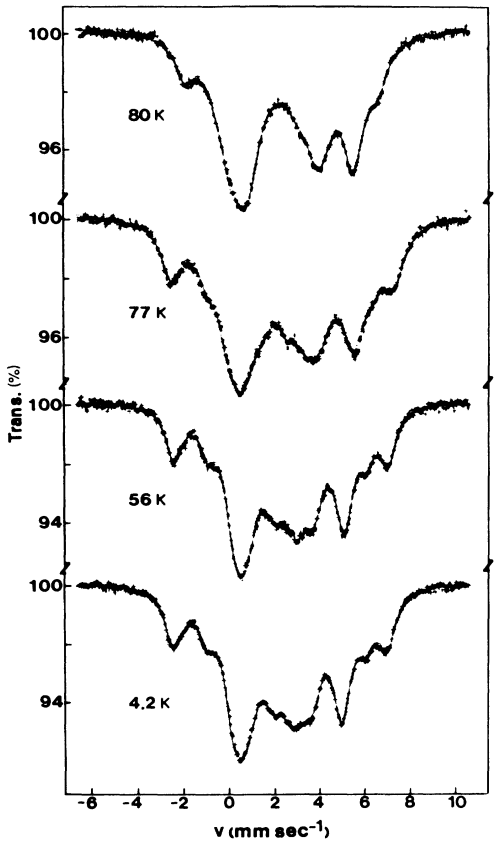

FIG. 6. ^{119}Sn Mössbauer spectra of $FeSn_2$ between 4.2 and 80 K. (The solid lines have been calculated with three sites, Sec. V B 2.)

step, we have simulated the resulting spectrum in order to evaluate the influence of these angles.

Only small differences exist between the spectra calculated either with a single site ($\theta_C = \theta_{C'}$) or with two sites as long as the difference between θ_C and $\theta_{C'}$ is not too great. This is illustrated by Fig. 7(a) where $\theta_C = \theta_{C'} = 28°$ (single site) and θ_C (or $\theta_{C'}$)$=41°$, $\theta_{C'}$ (or θ_C)$=15°$: the spectra are almost undistinguishable. The differences are more visible in Fig. 7(b) where $\theta_C = \theta_{C'} = 23.5°$ (single site) and θ_C (or $\theta_{C'}$)$=46°$, $\theta_{C'}$ (or θ_C)$=1°$. In both examples we have used $H_0 = 32.5$ kG.

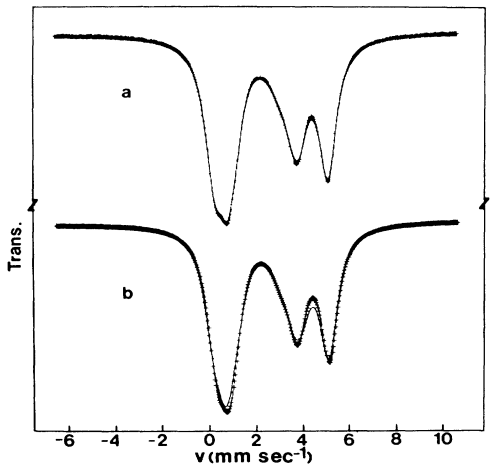

FIG. 7. ^{119}Sn Mössbauer spectra calculated for sites C and C'. (a) Crosses: $\theta_C = \theta_{C'} = 28°$; solid line: $\theta_{C'} = 15°$, $\theta_C = 41°$. (b) Crosses: $\theta_C = \theta_{C'} = 23.5°$; solid line: $\theta_{C'} = 1°$, $\theta_C = 46°$.

We conclude that the unique angle θ, that leads to the single site spectrum, best fitting the two sites spectrum must be chosen nearly equal to the mean value $(\theta_C + \theta_{C'})/2$ [Eq. (7)]. Mössbauer spectra fits have also been performed with a four tin site model, the calculated hyperfine fields are almost identical in both cases while the magnitude for the angles θ_C and $\theta_{C'}$ agrees well with our previous conclusions. The hyperfine parameters are reported in Table IV which demonstrates that magnetic structure II[a] allows fitting (χ^2) to the spectra recorded

TABLE IV. ^{119}Sn hyperfine parameters below $T_t = 93$ K. H is the hyperfine field, δ is the isomer shift with respect to $BaSnO_3$ at room temperature, $\Delta p = |\Delta(1+\eta^2/3)^{1/2}|$ where Δ is the quadrupolar splitting and η the asymmetry parameter, I gives the proportion of each site, and θ is the angle between H and V_{ZZ}. The domains of θ have been calculated using the Karyagin method as described in Refs. 2 and 3.

T (K)	Sites	I	H (±1 kG)	θ (deg)	δ (±0.02 mm s^{-1})	Δp (±0.02 mm s^{-1})	χ^2
4.2	1	0.29	66.5	89(1)	2.30	0.86	1.16
	2	0.23	4	35(3)			
	c	0.48	32.5	24(4)			
56	1	0.26	65	88(2)	2.32	0.82	1.03
	2	0.23	4	58(1)			
	c	0.51	32	22(3)			
77	1	0.29	59	87(3)	2.30	0.82	1.19
	2	0.21	8	83(7)			
	c	0.50	32	24(5)			
80	1	0.25	51	85(5)	2.29	0.84	1.06
	2	0.25	18	89(1)			
	c	0.50	31	23(4)			

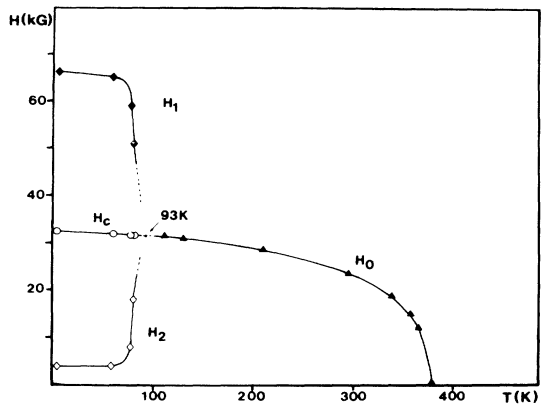

FIG. 8. Temperature dependence of the ^{119}Sn hyperfine fields (Sec. V C and Table IV).

below T_t (Fig. 6). The quadrupolar splitting Δp which is determined without ambiguity from such powder spectra, is within experimental error equal to the value measured above T_t^2: $\Delta p = 0.86 \pm 0.02$ mm s^{-1} whatever the temperature. The angle θ_2 (Table IV) must be considered with care as the corresponding field is small. As expected, the relative properties are close to 0.25:0.25:0.50. The hyperfine fields vary only slowly between 0 and ~ 70 K and rapidly between ~ 70 K and T_t (Fig. 8). We also note that the sum $H_1 + H_2$ is very close to $2H_C$ (Table IV).

C. Discussion

In Table V are reported the variations of the hyperfine fields H_A and H_B, calculated as a function of β with Eqs. (2)–(5), several values of h_{iso} and α ($< \alpha_{max}$, see Sec. V B 1) have been successively used ($\mu = 1.70 \mu_B$).

First, Table V shows that, for $|h'_{iso}| \simeq (30$ to 60 kG$)\mu_B^{-1}$, the hyperfine fields H_A and H_B have correct orders of magnitude (Table IV) thus to sites 1 and 2 of Table IV correspond the sites B and A, respectively. The maximum variation of $|H_B|$ (< 7 kG whatever α and h_{iso}), as a function of β for fixed values of α and h_{iso} is much less than the observed variation of H_B between ~ 70 K and T_t [$\simeq 14$ kG (Table I)] even if one takes into account the small variation of the magnetic moment μ, from $1.70\mu_B$ at 4.2 K to $\sim 1.68\mu_B$ at 77 K.

From Table V, we see that we can account for the temperature dependence of the experimental fields (Fig. 8) in various ways, for example, if (1) h'_{iso} is temperature independent and α decreases when T increases; (2) $|h'_{iso}|$ decreases when T increases and α remains approximately constant. As h'_{iso} is expected to be temperature independent, as in $MnSn_2$ (Ref. 3) for which h_{iso} and A_a do not vary with T, we retain solution (1) (see below). In fact, A_a is also temperature independent in $FeSn_2$. Finally, $\alpha \simeq 28°$ and $\beta = 0°$ at 4.2 K, whether $h'_{iso} \simeq -(50$ kG$)\mu_B^{-1}$ or $h'_{iso} \simeq (30$ kG$)\mu_B^{-1}$ (Table IV).

Under these conditions [solution (1)], the angle β must increase between ~ 70 K and T_t in order to satisfy Eq. (12) which was deduced from ^{57}Fe Mössbauer spectroscopy, as the ratio r is practically the same at 4.2 and 80 K (see Sec. V B 1).

The canting angle α is thus in agreement with $\alpha = 19 \pm 7°$ from neutron diffraction data. Moreover, from Eq. (8), $\theta_C \simeq \theta_{C'} \simeq \alpha$ agrees with the experimental value ($\theta_C = 24° \pm 4°$, Table IV).

In addition, the angle β calculated from Eq. (12) increases rapidly when α decreases. For example, $\beta = 0°$ for $\alpha = 28°$, $\beta = 22°$ for $\alpha = 20°$, and $\beta = 27°$ for $\alpha = 10°$. Consequently, β is likely to be of the order of 25° above ~ 70 K. This is again in agreement with the experimental angle θ_C which [Eq. (8)] is of the order of β (see Sec. V B 2) in this temperature range: $\theta_C = 23° \pm 4°$ at 80 K (Table IV).

We therefore propose the following qualitative description of the evolution of the magnetic structure of $FeSn_2$ when the temperature decreases from T_N to 4.2 K.

1. *Between T_N and $\sim T_t$*

$FeSn_2$ has a collinear antiferromagnetic structure. The spin direction deviates from $[100]_{cc}$ when T decreases and makes an angle of about 26° with $[110]_{cc}$ at T_t.

2. *Between T_t and ~ 70 K*

Close to T_t, the canting α is small (Tables IV–VI) and β is also of the order of 26°. When T decreases the direction of the canting propagation vector turns toward the $[110]_{cc}$ axis and α increases. Unfortunately we had recorded only one neutron diffraction pattern in this tem-

TABLE V. ^{119}Sn hyperfine fields H_A and H_B for some values of α, β, and h'_{iso}.

		$\alpha = 28°$		$\alpha = 10°$	
$\mu_B h'_{iso}$ (kG)	β (deg)	H_A (kG)	H_B (kG)	H_A (kG)	H_B (kG)
−60	0	12.1	69.4	16.9	47.1
	28	18.4	62.5	21.6	44
−30	0	11	46.3	25.4	38.5
	28	10.6	46.8	25.3	38.7
0	0	23.6	34	30	34
	28	30.8	39.4	30.9	34.7
30	0	0.2	57.2	21.4	42.5
	28	44.4	53.4	32.5	37.7
60	0	22.9	80.3	12.9	51.1
	28	58.9	76.4	32.5	45.1

TABLE VI. ^{119}Sn calculated parameters from comparison between model II[a] (Sec. V B 1) and experiment (Table IV).

T (K)	$\mu_B h'_{iso}$ (kG)	α (deg)	β (deg)	$\lvert H_A \rvert$ (kG)	$\lvert H_B \rvert$ (kG)	θ_B (deg)	
4.2	38	28	0	8.3	63.3	88	$h'_{iso}>0$
56	37	28	7.7	0	62.1	88	
77	35	28	0	6.6	59.9	88	
80	26	26	13	19.8	51.1	83	
	(37)	(18.5)	(23)	(31.1)	(49)	(82)	
4.2	−53	28	0	6.9	64	88	$h'_{iso}<0$
56	−52	28	0	6.1	62.8	88	
77	−54	25	15	7.8	59.3	82	
80	−75	13	26	17.6	51.2	78	
	(−53)	(17.5)	(24)	(14.2)	(50.1)	(76)	

perature range, close to the lowest limit ($T=72$ K). Nevertheless, we have "*a posteriori*" calculated the influence on the magnetic intensities of such an angle β for discrete values: $\beta=5°, 10°, \ldots, 30°$ ($\alpha=20°$). It results that the powder diffraction technique would not allow checking that β differs from zero as it has been deduced from Mössbauer spectroscopy performed at 77 and 80 K: no significant difference appears on the calculated structure factors for β varying from 0° to 30°.

3. *Below ~70 K*

The direction of the canting propagating vector is close to $[110]_{cc}$ and α is about 28°. This agrees well with the neutron diffraction results (Sec. IV). It is possible to perform a calculation [Eqs. (3)–(6)] of the order of magnitude of h'_{iso}. Equation (12) and the experimental fields H_1 (H_B) and H_2 (H_A) can be used to deduce the three unknown parameters α, β, and h_{iso}. Fixing α,β is deduced from Eq. (12) and h'_{iso} is calculated so that the sum of the squares of the difference between the calculated and experimental fields is minimum. Then, α is varied until a minimum of the previous sum is reached. Good fits to experiment are obtained for $h'_{iso}\simeq -(54\text{ kG})\mu_B^{-1}$ or $(37\text{ kG})\mu_B^{-1}$. In both cases, h'_{iso} is almost independent of T while α decreases and β increases at 80 K. For $T=80$ K, we have also given in Table VI the values of α, β, $\lvert H_A \rvert$, $\lvert H_B \rvert$, and θ_B (in brackets) assuming h'_{iso} to be equal to the mean value obtained for $T<77$ K: the calculated fields are closer to the experimental values for $h'_{iso}<0$ than for $h'_{iso}>0$. As already discussed in Ref. 3, h_{iso} is more likely to be negative. However, it is not possible to conclude unambiguously in favor of $h'_{iso}<0$ in the present work.

The values of α and β so obtained confirm the previous qualitative description (Table VI). Using Eq. (6) we have also calculated the angle θ_B for a $[110]_{cc}$ direction on the z principal axis of the EFG tensor. (The perpendicular direction gives values of θ_B in disagreement with experiment.) θ_B varies from 88° to 78° when T increases from 4.2 K to 80 K. The experimental angle shows the same trend (θ_1, Table IV).

Similar calculations have been performed with structure II[b]. They lead to identical conclusions for the magnetic structure changes with temperature and for the variations of α and β [Fig. 3(b)] with T. The required values of h'_{iso} are of the order of $-(10\text{–}10\text{ kG})\mu_B^{-1}$. Such a structure is also capable of explaining the ^{119}Sn Mössbauer spectra but, as seen in Sec. IV, it disagrees with neutron diffraction and will not be further discussed.

VI. CONCLUSION

Neutron diffraction and a hyperfine field model related to the nature of the chemical bond between the tin and $3d$ transition metal, successfully used in $MnSn_2$, have allowed determining unambiguously the low-temperature magnetic structure of $FeSn_2$ from among the two magnetic structure models which are consistent with the neutron diffraction data and the two which are consistent with ^{119}Sn Mössbauer spectroscopy. Below 93 K, the magnetic structure is noncollinear antiferromagnetic, the canting propagation vector is in the basal plane with a canting angle of ~28°, at 4.2 K, between the magnetic moment direction and the [110] direction of the chemical cell.

ACKNOWLEDGMENTS

This work has been carried out thanks to the support of the Centre National de la Recherche Scientifique (unités associées n° 158 et 159) and the Université Scientifique, Technologique et Médicale de Grenoble (France). We are indebted to the Institute Laue Langevin for the provision of research facilities. We thank M. P. Delcroix for recording some of the Mössbauer spectra.

[1]G. Venturini, D. Fruchart, J. Hübsch, G. Le Caër, B. Malaman, and B. Roques, J. Phys. F **15**, 427 (1985).

[2]G. Le Caër, B. Malaman, G. Venturini, D. Fruchart, and B. Roques, J. Phys. F **15**, 1813 (1985).

[3]G. Le Caër, B. Malaman, G. Venturini, and I. B. Kim, Phys. Rev. B **26**, 5085 (1982).

[4]E. E. Havinga, H. Danasma, and P. Hokkeling, J. Less-Common Met. **27**, 169 (1972).

[5]B. Malaman and G. Venturini (unpublished).

[6]J. B. Forsyth, C. E. Johnson, and P. J. Brown, Philos. Mag. **10**, 713 (1964).

[7]G. Le Caër, B. Malaman, G. Venturini, H. G. Wagner, and U. Gonser, Hyperfine Interact. **28**, 631 (1986).